New Laser-Based and Imaging Methods for Studying the Dynamics of Molecular Collisions

Paul L. Houston

Department of Chemistry, Cornell University, Ithaca, New York 14853-1301

Received: January 9, 1996; In Final Form: March 25, 1996[⊗]

The application of a wide variety of new techniques to studies of collision dynamics has changed our understanding of how molecular processes depend on such parameters as the initial state of reactants, the internal state of products, and the distance and angle of approach between two reactants. This article reviews the new techniques and places emphasis on those that allow the final velocity distribution of products to be determined of a function on the above-mentioned parameters.

I. Introduction

Although a knowledge of thermodynamics might indicate how far a chemical system is from equilibrium, it offers no clue as to how fast equilibrium will be approached. It is thus not surprising that teachers introduce the field of chemical kinetics at a very early stage in the education of a young chemist, usually by discussing the Arrhenius expression for the rate constant: $k(T) = A \exp(-E_a/RT)$, introduced just seven years before the birth of *The Journal of Physical Chemistry*. We go on to describe at a later time in a chemist's training how this simple expression might be understood in terms of either collision theory or activated complex theory. In a sense, the entire venerable history of chemical kinetics can be interpreted as an attempt to understand this equation in finer detail and to determine which features of the potential energy surface are most responsible for determining the rate constant.

A starting point for a deeper understanding of the rate constant is the recognition that both reactants and products have individual quantum states and that the thermal rate constant is obtained from the "state-to-state" energy-dependent rate constants by first averaging over both the Boltzmann-weighted initial states of reactant molecules and the collision energy and then summing over the final states of the products. The state-to-state rate constants are important in understanding a variety of interesting phenomena, including chemical lasing.[1] If each of the state-to-state rate constants is written in terms of collision theory, then we obtain $k_{if}(E_r) = \sigma_{if}(E_r)v_r$, where σ_{if} is the state-to-state cross section, "i" is the initial state, "f" is the final state, v_r is the relative velocity, and $E_r = {}^1/_2\mu v_r^2$ is the collision energy, proportional to μ, the reduced mass of the two colliding molecules.

Our next job, then, in "unaveraging" the thermal rate constant is to understand $\sigma_{if}(E_r)$, the energy dependent cross section for reaction between specified initial and final states. But even for a specified collision energy, $\sigma_{if}(E_r)$ is itself an average; it will depend both on the impact parameter for the collision, b, which describes how close the centers of the two reacting molecules would come if the forces between them did not alter their direction of approach, and also on the angles, which we will symbolize by γ, that collectively describe the orientation of each of the reactants with respect to their relative velocity. Thus, the state-to-state cross section at a more fundamental level can be written as $\sigma_{if}(E_r,b,\gamma)$. By specifying and varying the parameters E_r, b, and γ, one can, in principle, achieve a much more direct connection between the experimentally measured cross section and the potential energy surface governing the motions of the atoms.

Actually, even more detail can be obtained at the experimental level. As shown in Figure 1 for a simple A + BC → AB + C reaction, the products will leave the collision in some angular region dω with respect to the incoming relative velocity. In fact, the angular distribution of the products, called the differential cross section, can tell us much about the mechanism of the reaction.[2−4] For example, forward scattering in the center-of-mass frame might indicate a stripping reaction, while backward scattering might indicate a rebound reaction. Symmetric forward−backward scattering is usually evidence for formation of a collision complex. Finally, we might also learn about how the reaction depends on the orientation of the reactants (the collective angles γ) or whether the rotation axis of the product AB is aligned relative to either the initial relative velocity or the final velocity.

So far, we have considered only bimolecular reactions, but photoinduced unimolecular reactions can be described at the same level of detail with only a few minor changes. The state-to-state cross section in this case depends on the photon energy, $h\nu$, the polarization direction of the dissociating light, the angle that the parent molecule makes with that polarization direction, and, of course, the initial and final states of the reactants and products.

The purpose of this article is to describe recently developed experimental techniques for determining as much detail as possible about rate constants for unimolecular and bimolecular reactions. By necessity, as we have just seen, this detail will require methods for studying state resolution,[5] for preparing oriented reactants and measuring the orientation of products, for controlling the relative velocity and energy, for determining differential cross sections, and even for restricting impact parameters. Other experimental techniques,[6−11] also useful in molecular dynamics but not touched on here, will be covered elsewhere in this volume.[12−15] Even for the experimental techniques that are covered here, the present article is not meant to be an exhaustive review of results; other reviews, referred to as necessary, will better serve that purpose. I will aim, instead, to show one or two examples that clearly illustrate the power of each new technique.

Many of the techniques covered in this article concern ways to measure the velocity of a state-selected product. The reason that this particular measurement is so important is that, through conservation of energy and linear momentum, it provides information about the undetected product. Consider, for example, a reaction of the type A + BCD → AB + CD and suppose that we measure the velocity distribution of a selected

[⊗] Abstract published in *Advance ACS Abstracts,* June 15, 1996.

S0022-3654(96)00131-1 CCC: $12.00

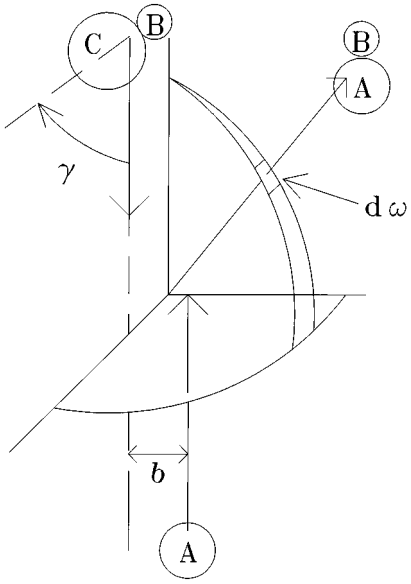

Figure 1. A + BC → AB + C as seen by an observer moving with center-of-mass of the ABC system. The product AB is scattered into a solid angle dω with respect to the initial relative velocity direction. The impact parameter is b, while γ symbolizes the collective polar and azimuthal angles of BC with respect to the relative velocity direction. The product C, not shown, recoils in a direction opposite to that of AB.

internal energy state of the AB product. By conservation of linear momentum, if we measure the AB velocity, we can then calculate the CD velocity and from it the total translational energy of the products. By conservation of energy, if the collision energy is well defined and if we know the change in energy for the bond rearrangement, then the measured total translational energy and the known internal energy of the AB product can be used to calculate the internal energy of the coincident CD product. It is this coincidence-like determination that makes the velocity of a state-selected product such an important quantity to measure.

I will thus begin the review with a discussion of methods for state-resolved velocity measurement. These fall into three categories: time-of-flight (TOF) methods, Doppler methods, and imaging methods. Subsequently, I will briefly touch on new procedures for better definition of the initial conditions: alignment of the reagents and restriction of the impact parameter distribution. Finally, I will cover direct investigation of the transition state region by spectroscopic techniques before concluding with a section that speculates on future directions.

II. Methods for State Detection and Product Velocity Measurement

A. Time-of-Flight Measurement of Product Velocities. Measurement of the time-of-flight of a product between two points in space is perhaps the most direct method for determining the velocity. Typically, one point in space is the origin of the reaction, for example, the intersection between two molecular beams or between a laser beam and a molecular beam. The second point is typically the spatial region of detection. If a product is made suddenly, for example by a short laser pulse, at the origin of the reaction, then the distribution of product arrival times at the point of detection is related to the distribution of product velocities. However, even if high time resolution is available and if these two points are defined with high spatial resolution, the precision of the velocity measurement will also depend on the reagent velocities, because the final product velocity will be a vector sum of its center-of-mass (COM) value with the laboratory velocity of the moving center-of-mass.

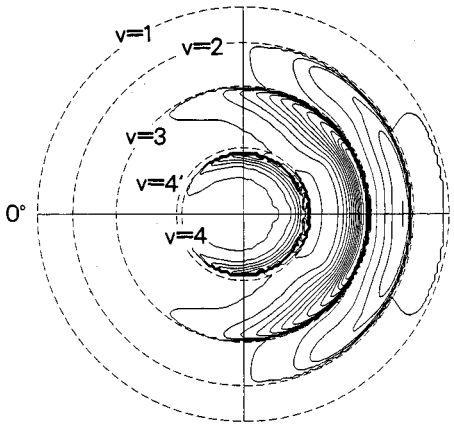

Figure 2. Differential cross section for the F + D_2 reaction at a collision energy of 1.82 kcal mol^{-1}. The contours show the DF velocity distribution. F atoms approach from the right (180°), while D_2 approaches from the left (0°). Reprinted with permission from ref 20. Copyright 1985 American Institute of Physics.

It is therefore very important experimentally to define the initial velocity distributions as narrowly as possible. Methods for achieving this goal have been discussed in detail elsewhere.[2−4,16−18] A typical technique is to use a supersonic expansion of the reactant of interest seeded in a rare gas. It is relatively easy by this method to obtain velocity distributions whose full width at half maximum is 10% of the center velocity. The average velocity of the distribution can be changed by adjusting the seeding ratio. These seeded beams have the further advantage that the expansion cools the reactant internal degrees of freedom so that the reactant is often left in a distribution favoring its lowest vibrational and rotational levels. A great deal of insight into both bimolecular and unimolecular reactions has been obtained by using such beams in conjunction with mass spectrometric detection.[2,3]

An example is the crossed-molecular beam reaction of F atoms with D_2.[5,19,20] A contour diagram giving the angular distribution of the DF product (the differential cross section) is shown in Figure 2. It was obtained by measuring the time-of-flight of the DF product at various angles with respect to the incoming crossed beams of F and D_2, which approach one another from the directions 180° and 0°, respectively. What can be learned from such a diagram? First, note the dashed circles superimposed on the diagram. These correspond to the maximum velocities in the center-of-mass frame consistent with the conservation laws for production of DF in various vibrational levels. (The center-of-mass point is at the center of the circles.) Because the unobserved D product in this reaction has a single quantum state, measurement of the DF velocity can be used to determine the DF internal energy. For example, the circle marked "$v = 1$" shows the velocity expected for DF(v=1,J=0). Higher rotational levels of this vibrational state would have less energy available for translation and so would lie within this circle. There are clear peaks in the contours near the energetic limits for the various vibrational levels, and these must then correspond to products formed in the indicated levels with varying amounts of rotational excitation. The contour peak for the $v = 3$ level is the highest, so most of the DF product must be formed in this state. Note that most of the product is scattered backward toward the incoming F atom. The reaction might thus be characterized as taking place via a "rebound" mechanism, at least at this collision energy.

A major source of uncertainty in any time-of-flight measurement results from the need to convert the laboratory measurement to the center-of-mass frame. Consider, for example, the separation of products R and X produced in a photodissociation

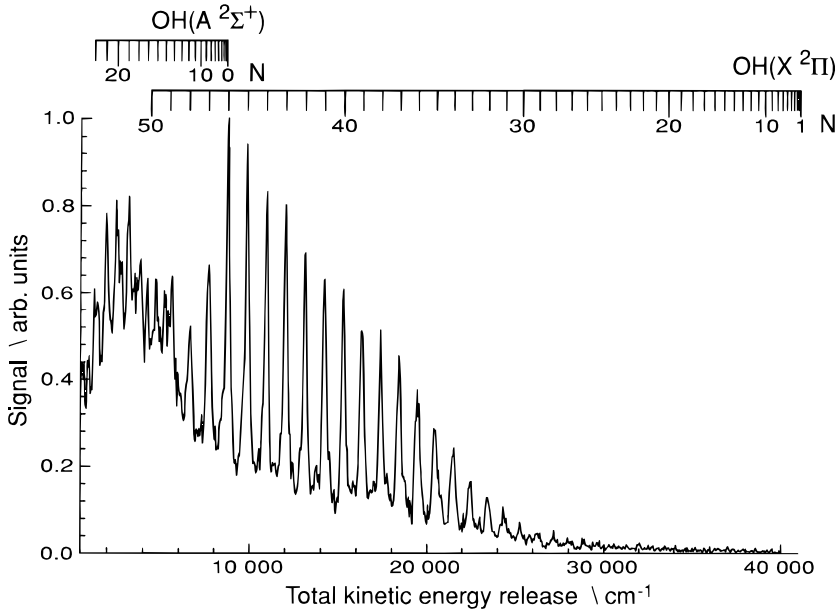

Figure 3. Total kinetic energy spectrum of the fragments resulting from 121.6 nm photodissociation of H_2O. Reprinted with permission from ref 29. Copyright 1991 Royal Society of Chemistry.

or bimolecular reaction, and suppose that the X fragment is detected at right angles to the RX center-of-mass velocity. Then

$$(v_{\mathrm{com(RX)}})^2 + (v_{\mathrm{lab(X)}})^2 = (v_{\mathrm{com(X)}})^2 \qquad (1)$$

where $v_{\mathrm{lab(X)}}$ is the observed laboratory velocity of X, $v_{\mathrm{com(RX)}}$ is the velocity of the RX center of mass, and $v_{\mathrm{com(X)}}$ is the velocity of X in the center-of-mass frame that we wish to determine. If X is an atom, then its velocity is related through the conservation laws of momentum and energy to the internal energy of R. It is thus of interest to see how accurately one might be able to determine $v_{\mathrm{com(X)}}$. In a typical TOF experiment, $\Delta v_{\mathrm{lab}}/v_{\mathrm{lab}}$ is fixed by the time resolution of the experiment and the distance through which X travels; it can typically be less than 1%. On the other hand, it is usual that $\Delta v_{\mathrm{com(RX)}}/v_{\mathrm{com(RX)}}$ is much larger, about 10%. From (1) we see that if $v_{\mathrm{lab(X)}}$ is large compared to $v_{\mathrm{com(RX)}}$, then $(v_{\mathrm{com(X)}})^2 \approx (v_{\mathrm{lab(X)}})^2$, or $\Delta v_{\mathrm{com(X)}}/v_{\mathrm{com(X)}} \approx \Delta v_{\mathrm{lab(X)}}/v_{\mathrm{lab(X)}}$; there will be no loss of resolution due to any spread in center-of-mass velocities of the parent RX. However, when $v_{\mathrm{lab(X)}}$ is small compared to $v_{\mathrm{com(RX)}}$, the percent uncertainty in $v_{\mathrm{com(X)}}$ is dominated by that in $v_{\mathrm{com(RX)}}$. For a given energy in translation, $v_{\mathrm{lab(X)}}$ will be high and about equal to $v_{\mathrm{com(X)}}$ when the mass of X is low, so it is for this situation that the time-of-flight technique will give the highest resolution. We therefore consider next the case when X is a hydrogen atom.

Welge and his collaborators have recently developed for hydrogen atoms an innovative TOF method that provides exquisite resolution for determining the energy distribution of the sibling product.[21−27] Although the technique has been applied to the photodissociation dynamics of many hydride molecules,[28] the case of H_2O photodissociation in the vacuum-ultraviolet illustrates its power.[29] Laser photons at 121.6 nm were used both to dissociate the molecular beam of H_2O and to excite the H atom products from $n = 1$ to $n = 2$. The atoms were further excited to levels with $n \approx 80$ by a second pulsed laser operating near 365 nm. A small electric field was used to repel any ions that might be formed. Although there is still some uncertainty as to the cause, apparently the H atoms in these large Rydberg orbits interact strongly enough with the residual gas and with the small electric field so that there is mixing among l and m values; large values of these quantum numbers are attained with the result that atoms have long radiative lifetimes. The time-of-flight of the Rydberg atoms was then measured from the point of intersection between the lasers and the molecular beam through a field-free region and to a particle multiplier located at right angles to the beams at a distance of 42.65 cm. As the atoms approach the particle multiplier, they became field-ionized by the high potential, and the resulting ions are accelerated into the detector. Because the perpendicular geometry was used and because the H atom velocity is much larger than the center-of-mass velocity, the experiment is insensitive to the spread in center-of-mass velocities, as discussed above. Furthermore, "tagging" the atoms by exciting them to high Rydberg levels rather than by ionizing them eliminates any spread in velocities due to ionic repulsion during the flight time. A review of photodissociation applications of this technique has recently appeared,[28] and another example is discussed elsewhere in this issue.[14]

Figure 3 shows the total kinetic energy release spectrum for the 121.6 nm photodissociation of H_2O along with a stick spectrum of OH(v=0) energy levels. It is apparent that individual rotational levels up to N =50 can be observed and that OH is produced both in its X ground state and in its A excited state. The OH is formed with little or no vibrational excitation. Previous investigations had been unable to determine the rotational distribution of the OH by laser-induced fluorescence because electronic excitation of these high levels leads to OH predissociation. The experiment thus provides the OH rotational distribution in both the *X* and *A* states and the branching ratio between the two electronic states. A close examination of the low kinetic energy release region led to the conclusion that there is some three-body dissociation.

A second example, this one for a bimolecular reaction, is provided by the Rydberg atom TOF study of the H + D_2 reaction.[5,19,30−32] The high resolution of the technique ($\Delta E/E$ = 0.5%) has been used to measure vibrationally and rotationally resolved differential cross sections. These have recently[32] been compared to quasiclassical trajectory (QCT) and quantum mechanical (QM) calculations on an *ab initio* potential energy surface.[33−35] The results, displayed for three laboratory scattering angles, are shown in Figure 4. There is essentially quantitative agreement between the experiment and the QM results and nearly as good agreement between the experiment

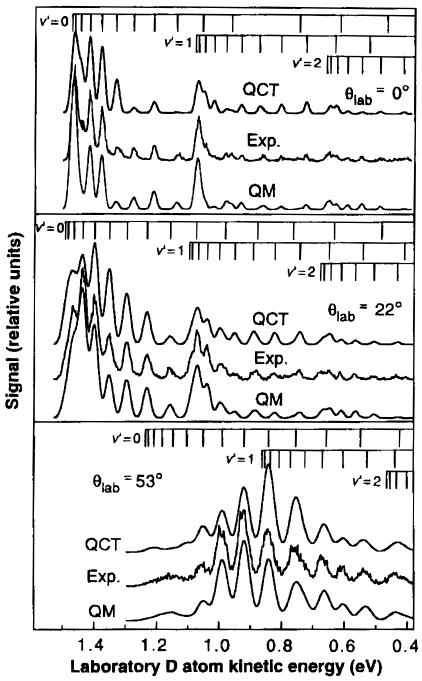

Figure 4. Laboratory D atom kinetic energy spectra at the indicated laboratory scattering angles θ_{lab} for the H + $D_2(v=0,J=0)$ reaction at a collision energy of 1.28 eV. The quantum mechanics and quasiclassical trajectory results are also shown. Reprinted with permission from ref 32. Copyright 1995 American Association for the Advancement of Science.

and the QCT calculations. Surprisingly, it was not necessary to consider explicitly the effects of geometric phase, recently proposed[36−39] to account for the discrepancy between previous experimental and theoretical results.[40−44] Further discussion of this reaction is provided in sections II.C and VI.

B. Doppler Measurement of Product Velocities. It is clear from these examples that a great deal can be learned from time-of-flight measurements, even when the detector does not restrict the product to a single state. The next goal, however, is to emphasize the additional detail that laser detection can furnish. For the velocity distribution to provide information about the undetected product, we need not only well-defined velocities and initial states but also state-specific detection. Two laser-based methods,[12−14] laser-induced fluorescence[45] and resonant multiphoton ionization,[46,47] are well suited to our needs. In each case, the signal is proportional to the density of molecules in the spectroscopically selected level, and the dependence of the proportionality on the identity of the level, typically involving a Franck−Condon factor and a rotational line strength, is known or can be approximated for many small product species. In each case the laser induces signal following excitation of a desired electronic and rovibrational transition of the product. In the former case, the signal is the total fluorescence intensity, integrated over wavelength, while in the latter case it is the total number of ions. Since the wavelength of the excitation laser is set to a particular spectroscopic transition, products in only the selected vibrational and rotational level are detected.

If the laser line width is narrow enough, then it will excite only those molecules in the selected internal energy level and also only those molecules which have the appropriate velocity component, w, along the direction of laser propagation. According to the first-order Doppler effect, the shift in absorption frequency, $\Delta\nu$, is given by

$$\frac{\Delta\nu}{\nu_0} = \frac{w}{c} \qquad (2)$$

where c is the speed of light and ν_0 is the absorption frequency for the molecule at rest. The power of the Doppler method is that by measuring the Doppler profile, $D(w)$, it is possible to obtain the velocity distribution of molecules in the selected internal state. If the velocities are isotropic and if molecules traveling in each direction are not aligned, then the Doppler profile is directly related to the speed distribution, $f(v)$;[48] it is essentially a one-dimensional projection of the three-dimensional velocity distribution onto a line parallel to the propagation direction of the probing light. Unfortunately, it is difficult to obtain $f(v)$ from $D(w)$ if the latter contains noise, so that it is usually a better procedure to guess $f(v)$ and compare iteratively a calculated Doppler profile to $D(w)$. Alternatively, one can fit a smoothed $D(w)$ to a truncated set of orthogonal polynomials and then obtain an approximation to $f(v)$ in terms of the fit coefficients and related functions.[49,50] It often occurs that the velocities are not isotropic and/or that molecules traveling at different angles have different alignments. For these cases, the Doppler profile, or usually several Doppler profiles taken under different experimental conditions, can be used to characterize not only the speed distribution but also both the anisotropy and alignment, as several excellent reviews have shown.[14,51−59] These points are illustrated by three examples.

The photodissociation of HI represents a case in which the velocities are not isotropic. When dissociated at 266 nm, HI absorbs light on a parallel transition to yield H + $I(^2P_{1/2})$ and on a perpendicular transition to yield H + $I(^2P_{3/2})$; the $I(^2P_{3/2})$ state is the ground electronic state of iodine, while the $I(^2P_{1/2})$ state lies about an electronvolt higher in energy. The Doppler profiles of the hydrogen atom products, monitored by vacuum−ultraviolet laser-induced fluorescence,[60] show clearly that the H atoms from the former channel have laboratory velocities directed principally along the polarization direction of the dissociating light, while those from the latter channel have velocities directed mostly perpendicular to that direction. The reason for this observation, as recognized first by Zare and Herschbach,[61,62] is that the dissociation laser preferentially excites those molecules whose transition dipole moment, μ, is along the polarization direction of the dissociating light field; the absorption varies as $\mu^2E^2\cos^2\theta$, where E is the strength of the field and θ is the angle between the transition dipole moment and the polarization direction. The transition dipoles of the excited molecules are thus initially aligned in the laboratory frame. The transition dipole moment always has a fixed direction in the molecular frame of reference. In the case of a diatomic molecule like HI, it is either parallel or perpendicular to the bond. If the molecules dissociate more rapidly than they rotate, then the repulsive force along the breaking bond will eject the fragments in a specific direction with respect to the transition dipole moment, and since the transition dipole moment is preferentially aligned in the laboratory frame by excitation with polarized light, the fragments can be expected to have an anisotropic laboratory velocity distribution.

In the HI case, H atoms associated with the $I(^2P_{1/2})$ channel would be expected to recoil in a direction parallel to the polarization because these are produced when the transition dipole is parallel to the bond, while those associated with the $I(^2P_{3/2})$ channel would be expected to recoil in a direction perpendicular to the polarization because these are produced when the transition dipole is perpendicular to the bond. When probed by light propagating parallel to the polarization direction of the dissociation laser, the H atoms from the former process will appear mostly in the wings of the Doppler profile, while those from the latter process will appear mostly in the center. The opposite conclusion holds when the probe light propagates perpendicular to the polarization direction. Since both processes

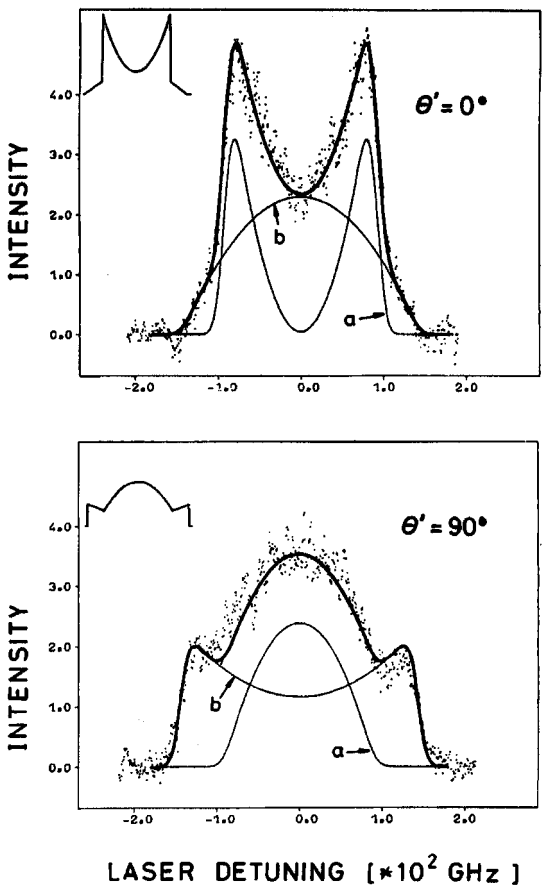

Figure 5. Experimental Doppler profiles (dots) measured with the polarization vector of the dissociation parallel to (top, $\theta' = 0°$) or perpendicular to (bottom, $\theta' = 90°$) the propagation direction of the probing laser. The solid curves marked (a) and (b) are the theoretical profiles for a pure parallel or perpendicular transition, respectively, and are weighted so that the sum yields the best fit to the data. The theoretical profiles expected under ideal resolution are shown in the upper left of each panel. Reprinted with permission from ref 60. Copyright 1982 Springer.

occur in the dissociation of HI, the resulting Doppler profiles are a composite that varies with the angle θ' between the polarization and propagation directions as shown in Figure 5, where "a" is the contribution from the I($^2P_{1/2}$) channel and "b" is that from the I($^2P_{3/2}$) channel.

Dissociations of polyatomic molecules are somewhat more complicated because the transition dipole moment is no longer restricted to be either parallel or perpendicular to the dissociating bond. Nonetheless, many anisotropic distributions have been measured from their Doppler profiles and interpreted to yield information about the direction of the dipole moment or about the lifetime of the dissociation event. Several reviews give an overview.[51−59] It is also worth mentioning that it is possible to use a time-of-flight mass spectrometer to record a one-dimensional projection of the velocity distribution as a distribution in arrival times.[63] Further experimental refinements allow a more direct determination of the speed distribution than that given by its one-dimensional projection. These use either a variant on the Doppler effect in which the products are allowed to expand before being probed[64−66] or a variant on the mass spectrometer technique in which only the ions along the flight axis are detected.[63] Caution should be exercised especially in using the mass spectrometer technique, since space−charge effects can produce speed distributions that are unphysical.

The Doppler profile will be further modulated if products moving in a particular direction have their rotation vector aligned with respect to their velocity vector.[67−71] The physical reason for this is can be understood on the basis of either classical or quantum mechanics. The efficiency of the probe process, involving as it does the absorption of light, will depend on the relative directions of the transition dipole moment for the *product* molecule and the polarization direction of the *probing* source. Consider product molecules moving in a particular direction and absorbing at a particular frequency within the Doppler profile. If these product molecules have their rotation vectors aligned with respect to their velocity vector, then their transition dipole moments will also be aligned. The average angle between these dipoles and the probe polarization will determine the absorption. Now consider product molecules moving in another direction and absorbing at a different frequency within the Doppler profile. Even if their rotation vectors are aligned in the same fashion with respect to their velocity vector as those of the first group, they will make a different average angle with the probe polarization so that their interaction with the probe light will be different than that of the first group. Thus, the efficiency of detection depends on angle of recoil or, equivalently, on the position of absorption within the Doppler profile. Put in quantum mechanical terms, the m_J distribution of the probed molecules depends on their Doppler shift, and since the absorption of polarized probe light depends on the m_J distribution, the Doppler profile will be affected by the alignment between product rotation and velocity vectors. One hallmark of a correlation between the velocity and rotational vectors is that fragment Q-branch transitions, for which in diatomics the transition moment is parallel to the rotation vector, will have different Doppler profiles than R- or P-branch transitions, for which the moment is perpendicular to the rotation vector.

One of the best-studied systems that demonstrates such alignment is the photodissociation of H_2O_2.[70,71,72−80] For room-temperature samples and dissociation at both 266 and 248 nm, the measured recoil anisotropy indicated that the fragments recoil in a direction perpendicular to the polarization of the dissociation laser; thus, the transition dipole moment is likely to be perpendicular to the O−O bond. Q-branch transitions were observed to have different Doppler profiles than P- or R-branch transitions. A careful analysis showed that the vector correlation between the recoil velocity and the rotational vectors of the OH fragment increased with rotational level and that the two vectors tended to be parallel rather than perpendicular. The interpretation of this result is that the dominant rotational motion of the OH fragment comes either from a torsion around the O−O bond or from parent rotation about an axis nearly parallel to this bond. More detailed summaries of this system have been provided elsewhere.[55,76,80]

Doppler techniques can be used to measure the velocity distribution of products of bimolecular reactions as well,[81−90] where the angular part of the distribution is known as the differential cross section (see Figure 1). These methods have been used for quite some time in conjunction with molecular beams, but it is only more recently that it has been realized that the Doppler profile of a state-resolved product contains information about the differential cross section, even for bulk, photoinitiated reactions.[91−111] This point is illustrated by recent work on the H + O_2 reaction, as discussed below.[100]

One way to generate atomic or radical reactants for the study of their subsequent reactions with other molecules is to photolyze a stable molecule; this often generates a reactive radical or atom with very high kinetic energy. Suppose that these photoproduced reactants have an isotropic distribution of velocity vectors and, further, that they subsequently react with

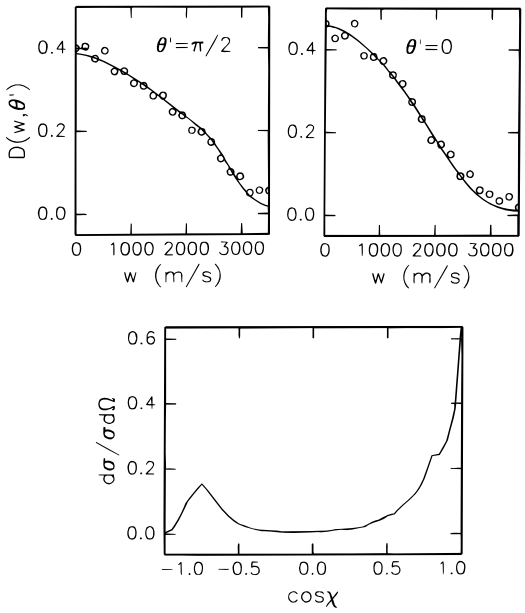

Figure 6. $P_1 17$ branch Doppler profiles taken in two different geometries (above) and the differential cross section that best fits both the Q-branch and P-branch profiles (below). Reprinted with permission from ref 100. Copyright 1994 American Institute of Physics.

a basically stationary collision partner to produce a product whose Doppler profile is then monitored. For any particular reactant direction, products scattered in the forward direction, as defined by the direction of the initial velocity of the fast reactant, will acquire a substantial laboratory velocity. The reason is that, under the stationary target assumption, the velocity of the center-of-mass of the reactant system is also moving in the forward direction; product velocities in the forward direction are added to this center-of-mass velocity to give the final laboratory velocity. By contrast, for products scattered in the backward direction the scattered velocity opposes the center-of-mass velocity, so that the product laboratory velocities will be smaller. Since the large product velocities corresponding to forward scattering produce a wide Doppler profile while the small ones corresponding to backward scattering produce a narrow profile, the width and shape of the Doppler profile are related in a simple fashion to the differential scattering cross section.

The top two panels of Figure 6 show Doppler profiles of the OH(v=0,J=17) produced by the H + O_2 reaction at a collision energy of 2.3 eV, while the bottom panel shows the form of the differential cross section that best fits not only this data, taken on a *P*-branch transition, but also data taken on a *Q*-branch transition (not shown).[100] The analysis also took into account the anisotropy of the H atoms, which were generated by the photodissociation of H_2S. The slight changes of the Doppler profile with geometry and excitation branch can be used to deduce that the reaction produces OH whose rotation vector is perpendicular to its velocity vector, at least for the $\Pi(A')$ lambda doublet component.

Doppler techniques or similar one-dimensional velocity projections using ion techniques continue to play an important role in understanding unimolecular and bimolecular processes both in beam and bulk samples. For example, a recent technique using opposing molecular beams provides a very simple way of obtaining a one-dimensional projection.[112−115] Another interesting application is to the dissociation of chiral molecules, where the vector correlations can, in principle, provide information about the "handedness" of rotation.[116−120] We will see in section VI how multiple one-dimensional techniques can be used to extract even more information from bulk sample reactions.

C. Imaging Methods for Measurement of Product Velocities. As discussed above, one-dimensional imaging of velocity distributions provides, in principle, information not only about the speed and direction of products but also about their angular momentum alignment. However, recovering this information often requires several different geometrical arrangements of the apparatus. Two-dimensional imaging techniques, while somewhat harder to set up initially, have the advantage that usually only one or two different geometrical arrangements suffice to determine uniquely the population and the alignment moments. Although methods for construction of the three-dimensional image from two-dimensional slices have been reported,[121−124] we will concentrate here on two-dimensional projection techniques. These techniques can be broadly classified into two main categories: noncoincidence measurements,[125] for which the data of a *single* product is recorded while integrating over all the states and identities of the sibling products, and coincidence measurements,[126,127] for which data on a *pair* of coincident fragments is recorded one pair at a time. The former technique has a decided advantage when the signal levels are high enough so that many product molecules can be detected on each repetition of the experiment, while the latter technique is more effective when the signal level is so low that at most one pair of products is detected on each repetition. In principle, both techniques can be used for either unimolecular or bimolecular reactions. A few recent review articles provide more technical details and examples.[128−130] We start by considering noncoincidence imaging of a unimolecular process.

Consider the photodissociation of a molecule like *trans*-dichloroethylene to produce CH_2CH_2Cl + Cl, where the chlorine atom can be in its ground spin−orbit state, which we will denote as Cl, or in its excited spin−orbit state, which we will denote as Cl*. Following earlier work,[131−133] the dissociation has more recently been investigated at 193 and 235 nm.[134] In the noncoincidence technique the dissociation products are actually detected as ions, and they are ionized by using a second laser to induce a process known as n + m resonant multiphoton ionization.[12] In this scheme, products in a spectroscopically selected initial state are first excited to an intermediate electronic state by n laser photons and then further excited by m more photons to the ionization limit. The Cl or Cl* atoms in this example are detected by 2 + 1 ionization near 235 nm. The ionization occurs immediately after the photodissociation, so that the fragments have not yet had a chance to fly out from their center-of-mass. Because the ejected electron has such small mass compared to the product, the velocity distribution of the product ions is nearly identical to the velocity distribution of the product neutrals. The products, now ions, are then allowed to expand with the velocities imparted from the initial photodissociation and are detected by accelerating them into a position-sensitive detector consisting of one or more microchannel plates. The electrons produced by ion impact in the channels are amplified as they travel through the plates and then accelerated to a phosphorescent screen. A digitizing camera then records the image for averaging and analysis. Although the image is a two-dimensional projection of the three-dimensional velocity distribution, the full three-dimensional information can be obtained by a straightforward mathematical manipulation.[128,129]

Figure 7 shows the images obtained for the Cl product of the dissociation at both 193 and 235 nm. Images for the Cl* product are qualitatively similar. At the former wavelength, the products are found near the center of the image, indicating that their speed distribution is peaked at relatively low values, while at the latter wavelength, the products are found on the

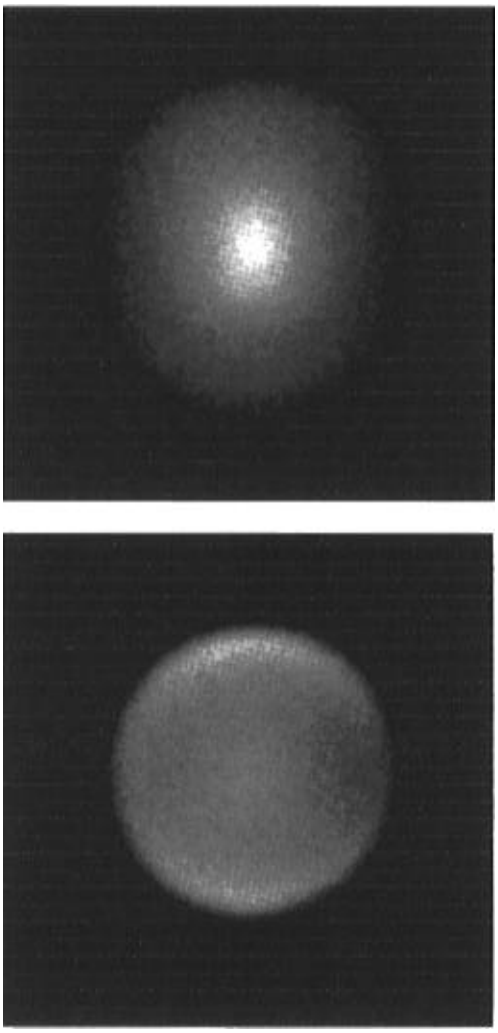

Figure 7. Images of the Cl observed in the 193 nm (top) and 235 nm (bottom) photodissociation of *trans*-dichloroethylene (from ref 134).

edge of the image, indicating higher speeds. The angular distributions are also quite different. While the 193 nm results are isotropic, products from the 235 nm dissociation are peaked at the top and bottom of the image in a direction basically parallel to the polarization direction of the dissociating light. Detailed analysis involves converting these two-dimensional projections of the velocities into the actual distribution using an Abel transform.[128,129] It is clear even from the projections, however, that dissociation at these two wavelengths proceeds by different mechanisms. A likely possibility is that the 193 nm dissociation is dominated by production of three fragments, $CH_2ClCH_2Cl + h\nu \rightarrow CH_2CH_2 + 2Cl$, whereas the 235 nm dissociation is dominated by production of two fragments, $CH_2ClCH_2Cl + h\nu \rightarrow CH_2CH_2Cl + Cl$.[135]

Imaging of bimolecular reactions by the noncoincidence technique has also been performed.[128,129] As an example, consider the $H + D_2$ reaction, already discussed in relation to Rydberg atom TOF techniques in section II.A. Figure 8 shows raw data images and their velocity distributions obtained at two collision energies.[138] In the upper panels, a beam of HI and a beam of D_2 are coming out of the plane of the image. The HI is photodissociated at 266 nm so that some H atoms are directed from the HI beam downward to the D_2 beam. The D atoms produced in the reaction are ionized and imaged. It is clear from the raw data in the top panels that the D atom products are scattered mostly in the forward direction, *i.e.*, along the initial H atom velocity. The actual distributions obtained by Abel transformation are shown in the middle row of panels, on which are superimposed circles, calculated using conservation of energy and momentum, that depict the radius within which D atoms formed in coincidence with various HD states should be located. The bottom panels show the differential cross sections obtained from analysis of the velocity distributions. As mentioned in section II.A, the product-state-summed differential cross section obtained in this work has been found to be in good agreement with the sum of the product-state-resolved differential cross sections obtained by Rydberg atom time-of-flight techniques.[32]

While the above examples use noncoincidence imaging, coincidence imaging has also been used to study molecular dynamics.[14] The method uses a novel detector that can register the position and arrival time of two coincident product molecules that are matched by conservation of momentum. Typically, a fast beam of neutral particles is photodissociated, the fragments strike a microchannel plate assembly, and the resulting electrons are accelerated into a "wedge and strip" detector divided into two halves.[137] If fragments arrive on the opposite halves within a chosen time window, their relative positions are determined to within about 100 μm by measuring the charge distribution at multiple anodes, and their relative arrival times are measured to within about 500 ps. The position and time information can be used to calculate the relative velocity between the momentum-matched fragments in the center-of-mass frame, and conservation of energy then permits an energy release spectrum of the products to be compiled from the averaged data. The resolution of the apparatus is greatly improved if the initial state of the dissociating parent is known. For example, if the fast neutrals are obtained by dissociative photodetachment of accelerated negative ions, photoelectron spectroscopy can serve to define the initial state. In fact, a photoelectron−neutral−neutral coincidence measurement on O_4^- has recently shown the power of this new refinement.[138,139] A drawback of these techniques is that at most one pair of fragments must be detected per repetition of the experiment, but the detailed information available outweighs this disadvantage as long as sufficient signal can be obtained.

While many dissociations have now been studied by this technique,[140−148] the example of O_2 perhaps best illustrates its power.[146] O_2^- was created in a pulsed ion source and accelerated to about 5 keV. The electron was then photodetached with a pulsed laser operating at 480 nm, and the resulting O_2, still moving at 5 keV, was photodissociated by exciting specific vibrational−rotational levels of the O_2 B $^3\Sigma_u^-$ state. These predissociate to give two $O(^3P_J)$ atoms, where J indicates the 0, 1, or 2 spin−orbit component. Each atom then strikes a microchannel plate, and the resulting electrons are detected on opposite halves of a wedge-and-strip detector. From their arrival times and positions, their recoil energy is determined to within 7−10 meV. This resolution is sufficient to yield the correlated fine structure distribution for the two atoms, *i.e.*, the probability $P(J_1,J_2)$ that one oxygen atom will be in the spin−orbit state J_1 when the other is in state J_2.

Imaging techniques are receiving increased attention in many branches of molecular dynamics. They are particularly important in gas−surface applications[149−154] and ion processes.[155] New imaging techniques promise to make this method even more versatile.[121−124,156−162]

III. Methods for Alignment and Orientation of Reactants

We saw in the Introduction that the differential cross section for a reaction could be written as a function of initial and final states, relative velocity, impact parameter, and angle of approach. The experiments we have considered so far, while

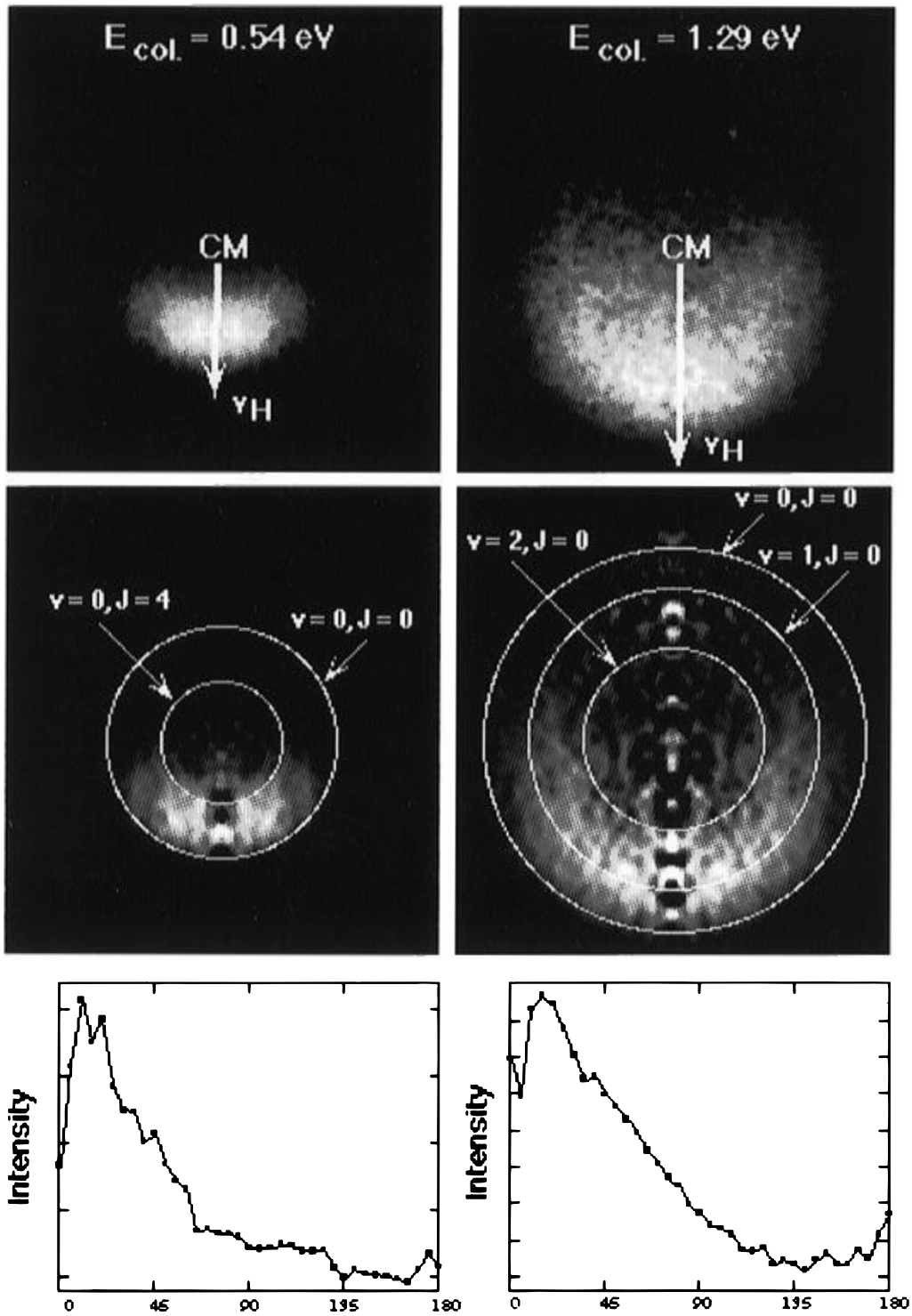

Figure 8. Images of D atoms formed in the reaction of H + D_2. The left and right columns are for collision energies of 0.54 and 1.29 eV, respectively, while the top, middle, and bottom rows show the raw data, the Abel transformed velocity distribution, and the differential cross section (intensity vs scattering angle), respectively. The center-of-mass and H atom velocities are indicated in the top row of panels. Reprinted with permission from ref 136. Copyright 1993 American Association for the Advancement of Science.

measuring the angular distribution of products for selected relative velocity and initial and final states, have averaged over both impact parameter and angle of approach. In this and the next section, we consider ways of unraveling this averaging. Several review articles[163−171] and journal issues[172−175] have concentrated on measurements that select the angle of approach. There are two common methods to achieve such alignment or orientation: optical excitation and use of electric fields.

The optical excitation method takes advantage of the properties of polarized light. For example, linearly polarized light excites transitions with $\Delta m_J = 0$, so that excitation of a vibrational−rotational transition from, say, $J = 0$ to $J = 1$ with linearly polarized light would produce a distribution of m_J levels in the $J = 1$ state in which only the $m_J = 0$ level is populated with no population in the $m_J = \pm 1$ levels. This distribution would thus be aligned in such a way as to prepare the **J** vector of the rotating molecule to be preferentially perpendicular to the polarization direction of the excitation source. An early experiment using such preparation investigated the reaction of Sr with aligned HF,[176] but was confounded due to nuclear spin coupling.[177,178] More recent investigations of the same reaction show that slightly more SrF(v=0) products are formed in end-

on rather than side-on collisions.[179] Many examples using polarized light to align atomic orbitals have also been reported.[169,170]

The electric field methods for orientation and alignment take advantage of the orientational energy of a dipole in an electric field. Note that because the dipole has distinct positive and negative ends, the molecule is not merely aligned so that its axis is parallel to the field, but also oriented so that one end of the molecule points preferentially in a specific direction. A problem must be overcome, however. Because molecules usually have rotational energy in excess of the dipole energy caused by the field, the dipole moment will usually precess about the rotation vector, greatly reducing any alignment or orientation. There are two ways to surmount the problem. One, sometimes called the "brute force" approach, is to prepare the reactant in a supersonic expansion molecular beam source, so that the rotational distribution of the reactant is cooled to a few degrees kelvin. Under these conditions, some of the population will be in states low enough to be "trapped" in so-called "pendular" states as the dipole enters a strong electric field.[180−182] Classically, the dipole angle with respect to the field oscillates, but on average the reactant is oriented along the field lines. A second way to overcome the problem of dipole precession is to prepare an individual $|JKM\rangle$ state of a symmetric top molecule, where J, K, and M are the quantum numbers specifying the rotation of the top. By symmetry arguments, the dipole moment in such a reactant must be along the top axis, and selection of an individual state specifies both the projection of the total angular momentum onto the field direction and its projection onto the top axis. The dipole moment still precesses about the field direction, but it will have a nonzero average orientation along that direction. A useful method for state selection is to employ a hexapole field, as reviewed elsewhere.[163,165−168] Orientation and alignment can often be verified by photodissociation of the aligned species and examination of the angular distribution of the products.[183−187]

Let us examine results from an orientation experiment in which the stereodynamics of the Rb + $CH_3I \rightarrow CH_3$ + RbI reaction were investigated at a rather low collision energy (around 0.1 eV).[165,188] A hexapole focusing field was used to state-select methyl iodide molecules before they passed into a region of linear electric field. It was thus possible to orient the methyl iodide, *i.e.*, to choose the value of $\langle\cos\gamma\rangle = KM/(J^2 + J)$, where γ is the angle of the C−I bond with respect to the relative velocity between Rb and CH_3I. As might be expected, the reaction Rb + $CH_3I \rightarrow$ RbI + CH_3, was found to be much more probable if the CH_3I were in the orientation with the I end pointed toward the Rb than if it were in the orientation with the methyl end toward the Rb. The results are summarized in Figure 9, which shows a "cone of nonreaction" centered on the methyl group with a width of about 53°.

In contrast to the cone of nonreaction found for low collision energies in the Rb + CH_3I reaction, Loesch and Remscheid found for the K + CH_3I reaction at higher collision energies (0.79−1.24 eV) that reaction took place for collisions striking either end of the methyl iodide, but that the differential cross section was considerably different for the two cases.[189,190] Their study used the brute force method; a supersonic expansion and a high electric field oriented about 2% the CH_3I reagent relative to the incoming beam of K atoms. If we denote β_L as the angle between the orienting electric field and the K atom beam direction, then the "steric effect" can be defined as

$$S(\Theta,\beta_L) = \frac{I_{LAB}(\Theta,\beta_L) - I_{LAB}(\Theta,\beta_L+180°)}{I_{LAB}(\Theta,\beta_L) + I_{LAB}(\Theta,\beta_L+180°)} \qquad (3)$$

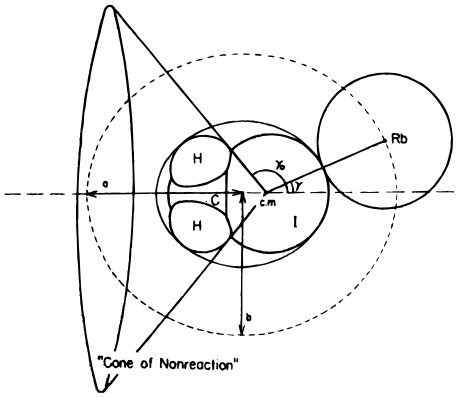

Figure 9. Pictorial representation of the steric aspects of the CH_3I + Rb reaction. Reprinted with permission from ref 188. Copyright 1985 American Institute of Physics.

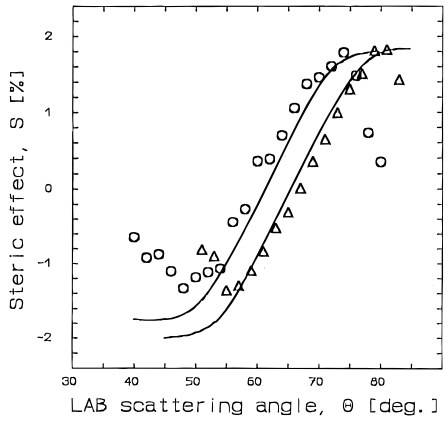

Figure 10. Angular variation of the steric effect for the collision of K with methyl iodide at two collision energies: 0.79 eV (triangles) and 1.24 eV (circles). The solid lines are a theoretical fit to the data. Laboratory angles less than about 60° correspond to scattering in the forward hemisphere, while those more than 60° correspond to scattering in the backward hemisphere. Reprinted with permission from ref 189. Copyright 1990 American Institute of Physics.

where Θ is the laboratory scattering angle. Figure 10 shows the steric effect at the two different collision energies. Note that the angle corresponding to the center-of-mass direction is about 60°, so that laboratory angles smaller (larger) than this correspond to scattering in the forward (backward) hemisphere. Two observations are important: (1) The maximum steric effect is about 2% and about equal to the fraction of CH_3I molecules that was oriented; thus the steric effect is significant. (2) Negative steric effects, corresponding to collisions with the CH_3 end of the methyl iodide, occur for products scattered to the forward direction, while positive steric effects, corresponding to collisions with the I end, occur for products scattered to the backward direction. The interpretation of this data is that, unlike the Rb + CH_3I reaction at lower collision energies, that of K with CH_3I at these energies takes place efficiently at both ends of the methyl iodide, but that collisions with the methyl end lead to stripping reactions whereas collisions with the I end lead to rebound reactions.

While it is not practical to review more than these few applications here, it should be noted that methods for orientation and alignment are becoming increasingly common in studies of molecular dynamics. Many more examples are given in recent reviews.[163−175]

IV. Methods for Impact Parameter Definition

It is clear from the above sections that new methods have made great advances in specifying the alignment of reactants,

in measuring the states and velocities of products, and in determining the vector correlations between products. State-resolved differential cross sections are now available for many processes. However, the previously discussed techniques have provided no method for controlling the impact parameter of the collision. One method for partially achieving this goal as well as for partially specifying the angle of approach is to start with the reactants in the equilibrium geometry of a van der Waals cluster. This field is an active one, not only because of what it tells us about the dynamics of bimolecular reactions but also because it offers insights into caging and recombination, processes of importance for studies of condensed phase reactions. Several reviews of the field have appeared,[191−198] so that we will concentrate here on a few representative examples.

A number of groups have investigated photodissociation of $HX{\cdot}CO_2$ complexes, where X = Br or I, as a way of learning about the combustion reaction $H + CO_2 \rightarrow OH + CO$. The idea of the experiment is to photodissociate the HX species in a complex that holds the HX in a restricted geometry relative to the other partner, CO_2 in this case. The H atom will then be directed toward a limited range of locations on the CO_2 molecule. It is known for the $HBr{\cdot}CO_2$ complex and assumed for the HI complex that the H atom is adjacent to the carbon atom with a O−C−H bond angle of approximately 90°,[199,200] although the zero-point amplitude is very large. The experiment, in principle, restricts both the impact parameter distribution and the distribution of angles of approach. The results of such studies, when compared to those in which the complete range of impact parameters and angles is sampled, show that there is much less energy deposited in the OH internal degrees of freedom when the reaction starts from a complex.[195,201] Although it was originally thought that the differences observed might stem from the limited range of impact parameters and approach angles, it now appears that the resulting HOCO complex actually decomposes statistically, but that less energy is imparted to HOCO when the reaction starts from a complex. The X atom takes away more energy in translation, leaving less for HOCO, because, to some extent, it pushes off from the entire HOCO complex rather than just from the lighter H atom.[198] Further evidence for the statistical nature of the HOCO breakup came from time-domain experiments.[202−208] The OH appearance rate was found to be in accord with the predictions of RRKM theory.[207,208]

Whereas the above experiments probed reactions on the ground electronic potential energy surface, it is also possible to probe excited state reactions by starting with the photodissociation of van der Waals clusters. An example is the reaction $Hg(6^3P_1) + H_2 \rightarrow HgH(^2\Sigma^+) + H$.[192,204] By using a supersonic expansion, it is possible to prepare a complex between ground state mercury atoms and H_2 in which the H_2 is freely rotating. When the complex is excited at wavelengths near the Hg-$(6^1S_0 \rightarrow 6^3P_1)$ transition, reaction is induced, but the time scale for reaction depends critically on the orientation of the excited mercury 6p orbital with respect to a line between the Hg and the center-of-mass of the H_2. Frequencies slightly lower than that of the Hg resonance line excite a $^3\Pi$ state of the complex for which the excited 6p orbital is perpendicular to the Hg−(H_2) bond. Reaction then proceeds rapidly by insertion of the Hg into the H−H bond, as evidenced by the lack of structure in the action spectrum of HgH emission induced by a probe laser tuned to the $HgH(^2\Sigma^+ \rightarrow {}^2\Pi_{1/2})$ transition. By contrast, frequencies slightly higher than that of the Hg resonance line excite a $^3\Sigma$ state of the complex, for which the excited 6p orbital is parallel to the Hg−(H_2) bond. Reaction proceeds more slowly than 3 ps, since there is structure in the action spectrum.

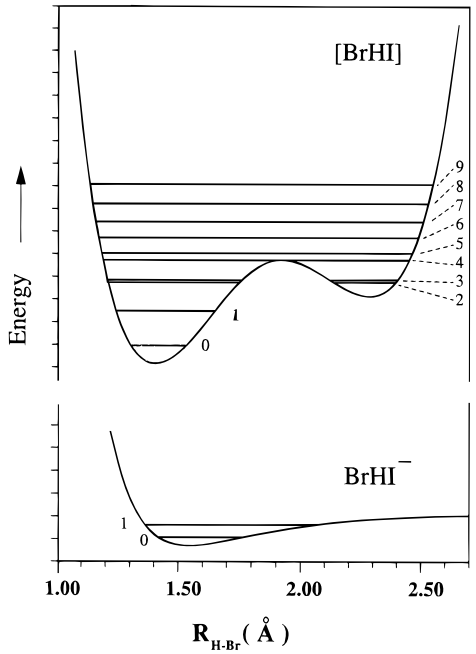

Figure 11. Anion and neutral ν_3 potentials of $BrHI^-$. Reprinted with permission from ref 212. Copyright 1990 American Institute of Physics.

V. Methods for Spectroscopy of the Transition State Region

We have seen above that more and more sophisticated methods for defining the reactants and measuring the products are becoming available. Although these methods have provided, in conjunction with sophisticated theory, the most detailed information we have to date about rate constants and the potential energy surfaces that control them, they probe only indirectly the transition state region. Negative ion photodetachment[209−211] has recently emerged as a method for direct, spectroscopic probing of this region, as can be illustrated by the example of BrHI.[212]

Figure 11 shows a one-dimensional cut along the H−Br distance through the calculated collinear potential energy surfaces for $BrHI^-$ and BrHI. Imagine that a beam of $BrHI^-$ ions, all in their ground vibrational level, is crossed with a pulsed laser beam at 213 nm. Photodetachment produces the neutral BrHI species plus an electron whose kinetic energy depends on the final state of the neutral. Peak positions in the photoelectron energy distribution then provide information about the level structure of the BrHI neutral, while peak intensities are governed by Franck−Condon factors between the initial state of the ion and the final state of the neutral. As long as the initial geometry of the ion is similar to that of the transition state for the Br + HI ⇌ BrH + I reaction, the method will provide direct information about this important region of the potential energy surface. For the system under consideration, the "vibrational levels" of the transition state region are metastable with respect to reactants or products and involve the ν_3 motion of the H atom between the heavier Br and I atoms, a motion which is much faster than the slower movement along the reaction coordinate involving lengthening of the distance between the Br and I atoms.

Figure 12 shows as dashed lines the photoelectron kinetic energy spectrum of $BrHI^-$ and $BrDI^-$ following ionization at 213 nm. The solid lines are a fit to a one-dimensional analysis

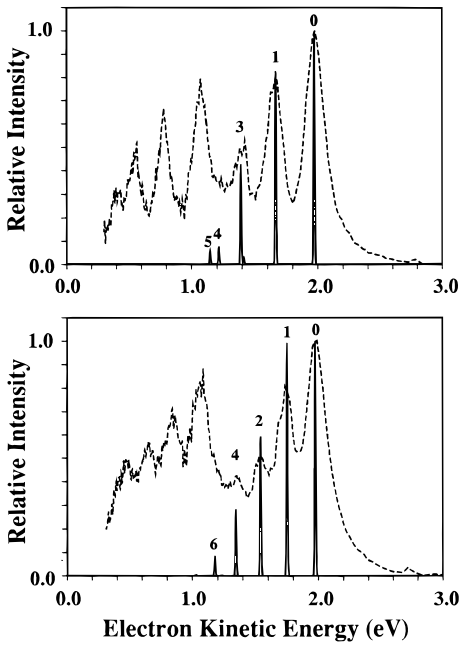

Figure 12. Experimental data (dashed lines) and calculated stick spectra for (top) $BrHI^-$ and (bottom) $BrDI^-$. Reprinted with permission from ref 212. Copyright 1990 American Institute of Physics.

based on the potential energy curves of Figure 11. Numbered assignments correspond to the ν_3 quantum number of the BrHI complex. The agreement between the positions and intensities of the assigned peaks and the experimental spectrum, already good, can be improved somewhat by using a more accurate two-dimensional wavepacket analysis.[212] The agreement lends confidence to the calculated potential energy surface upon which the simulated spectrum is based. Note that not all peaks in the experimental spectrum are assigned and that the pattern of unassigned peaks at lower electron kinetic energy is quite similar to that of the assigned peaks. It is thought that these lower kinetic energy peaks involve photodetachment to an electronically excited state of BrHI that would correspond to production of HBr in coincidence with the excited iodine atom $I(^2P_{1/2})$ rather than the ground state atom $I(^2P_{3/2})$.

The negative ion photodetachment method has been applied to a large number of systems.[209−211] In the case of FHH,[213,214] for example, the outstanding agreement between the experimental spectrum and three-dimensional quantum mechanical calculations on a new *ab initio* potential energy surface served to establish that the minimum energy path for this reaction is not through the collinear geometry.

VI. The Future

A major trend for future studies of reaction dynamics will be the increased use of laser and Doppler based methods of preparation and analysis, already presaged in 1978.[215] Doppler techniques are now being used routinely[56−58] to study the velocity dependence of collisional processes.[25,216−226] For example, using an elegant Doppler technique first introduced by Smith *et al.*,[220] absolute cross sections as a function of velocity have recently been obtained for an inelastic process involving rotational energy transfer in $Xe-Li_2$ collisions.[25,227] By using a two-photon excitation scheme with sub-Doppler resolution and lasers that propagate at right angles to one another, it is possible to select two laboratory velocity components of an Li_2 molecule in a prepared vibrational−rotational level of an upper electronic state.[227] Since Li_2 moves much more rapidly than Xe, these selected components also specify the center-of-mass velocity. Emission from levels created by collisions can then be used to study how the collisional energy transfer depends on the relative velocity. Alternatively, by using one photon to prepare the initial state and a two-photon process to monitor the final state, it is possible to obtain *differential* cross sections as a function of the initial velocity.[25] Similar two-photon techniques using circular dichroism can provide even higher-order measurements, such as the four-vector correlation between the angular momentum and relative velocity alignments before and after the collision.[228]

Reactive processes have also been probed using a variety of multiple one-dimensional preparation and analysis techniques, including Doppler preparation and one-dimensional ion imaging.[96,100,229−243] A particularly nice example is the measurement of the state-specific differential cross section for the $H + D_2 \rightarrow HD(v=4,J=3)$ reaction at a collision energy of 2.2 eV,[238] a reaction whose general features have already been discussed in some detail in sections II.A and II.C. Photodissociation of HI was used to initiate the process. After about 20 ns, a probe laser excited the $HD(v=4,J=3)$ products to a high Rydberg level. By choosing the center of the Doppler profile for this excitation, the Rydbergs were created with a nearly zero velocity component along the *x* direction, defined as the propagation direction of the probe laser. After 600 ns, the Rydbergs were field ionized, and the resulting ions were injected into a time-of-flight mass spectrometer, operated in such a way as to be sensitive to the positions and velocities of the original ions.[63] By using a slit-shaped mask, it was possible to select the products with nearly zero velocity component in the *y* direction. Thus, the products had nearly zero velocity in both the *x* and *y* directions, and the velocity in the *z* direction was measured using the time-of-flight apparatus. Analysis shows that the differential cross section for this particular reaction channel has two broad peaks centered around 75° and 140°.

One can easily speculate on where such experiments might lead in the future. First, it would be easily possible to choose one velocity component with the probe laser and to measure two components of the velocity distribution simultaneously using an imaging technique.[125] In addition, the probe laser undoubtedly can be used to measure a component of the rotational alignment at the same time, as already discussed in section II.B. Now suppose that the attacking radical is a diatomic AB rather than a hydrogen atom. One might, by photodissociation of ABX $\rightarrow$ AB + X, with X and atom, produce the diatom with a very narrow speed distribution. Using one laser to excite AB, it would then be possible to choose the initial vibrational and rotational state while simultaneously selecting a particular direction for the velocity, via the Doppler effect, and an anisotropic alignment, via the laser polarization. The result would be an experiment where one could obtain information on the differential cross section with partial alignment of the reactants, complete state selection, and partial analysis of the product alignment, all using existing laser techniques and without the need for a molecular beam.

A century has now passed since Arrhenius proposed the temperature-dependent form for molecular rate constants. Although we can claim to understand how to unravel this rate constant into its component parts for some simple bimolecular reactions and for a variety of unimolecular ones, we can claim neither to understand any reaction completely nor to understand many reactions at the level of, for example, $H + H_2$ or $F + H_2$. In its second century, *The Journal of Physical Chemistry* can confidently be predicted to be a forum for a deeper understanding of a wider variety of reactions as newly developed experimental techniques come to full fruition.

Acknowledgment. I gratefully acknowledge support during the preparation of this article by the National Science Foundation under Grant CHE-9531705 and by the Department of Energy under Grant DEFG02-88ER13934.

References and Notes

(1) Polanyi, J. C. *Angew. Chem.* **1987**, *99*, 981−1001; *Chem. Scr.* **1987**, *27*, 228−247; *Science* (*Washington, D.C.*) **1987**, *236*, 680−690.
(2) Hershbach, D. *Chem. Scr.* **1987**, *27*, 327−47; *Angew. Chem.* **1987**, *99*, 1251−75.
(3) Lee, Y. T. *Science* **1987**, *236*, 793−8; *Angew. Chem.* **1987**, *99*, 967−80; *Chem. Scr.* **1987**, *27*, 215−28.
(4) Bernstein, R. B. *Chemical Dynamics via Molecular Beam and Laser Techniques*; Oxford University Press: New York, 1982.
(5) See also in this issue: Moore, C. B.; Smith, I. W. M. State-resolved Studies of Reactions in the Gas Phase. *J. Phys. Chem.* **1996**, *100*, 12848.
(6) Gaubatz, U.; Rudecki, P.; Schiemann, S.; Bergmann, K. *J. Chem. Phys.* **1990**, *92*, 5363.
(7) Schiemann, S.; Kuhn, A.; Steuerwald, S.; Bergmann, K. *Phys. Rev. Lett.* **1993**, *71*, 3637.
(8) Dittmann, P.; Pesl, F. P.; Martin, J.; Coulston, G. W.; He, G. Z.; Bergmann, K. *J. Chem. Phys.* **1992**, *97*, 9472.
(9) Butenhoff, T. J.; Rohlfing, E. A. *J. Chem. Phys.* **1993**, *98*, 5460.
(10) Butenhoff, T. J.; Rohlfing, E. A. *J. Chem. Phys.* **1993**, *98*, 5469.
(11) Wasserman, T. A. W.; Arias, A. A.; Kandel, S. A.; Hsu, D.; Vacccaro, P. H. *Proc. SPIE* **1995**, *2548*, 220.
(12) See also: Zare, R. N. Lasers and Applications. *J. Phys. Chem.* **1996**, *100*, xxxx.
(13) See also in this issue: Zewail, A. H. Femtochemistry. *J. Phys. Chem.* **1996**, *100*, 12701.
(14) See also in this issue: Butler, L. J.; Neumark, D. M. Photodissociation Dynamics. *J. Phys. Chem.* **1996**, *100*, 12801.
(15) See also in this issue: Bowers, M.; McLaffrerty, F.; Marshall, A. Recent Breakthroughs in Mass Spectrometry. *J. Phys. Chem.* **1996**, *100*, 12897.
(16) Smalley, R. E.; Levy, D. H.; Wharton, L. *J. Chem. Phys.* **1976**, *64*, 3264.
(17) Scoles, G. *Atomic and Molecular Beam Methods*; (Oxford University Press: New York 1988.
(18) Levine, R. D.; Bernstein, R. B. *Molecular Reaction Dynamics and Chemical Reactivity;* Oxford University Press: New York, 1987.
(19) See also in this issue: Schatz, G. C.; Scattering Theory and Dynamics: Time-Dependent and Time-Independent Methods. *J. Phys. Chem.* **1996**, *100*, xxxx.
(20) Neumark, D. M.; Wodtke, A. M.; Robinson, G. N.; Hayden, C. C.; Shobatake, K.; Sparks, R. K.; Schafer, T. P.; Lee, Y. T. *J. Chem. Phys.* **1985**, *82*, 3067.
(21) Biesner, J.; Schnieder, L.; Ahlers, G.; Xie, X.; Welge, K. H.; Ashfold, M. N. R.; Dixon, R. N. *J. Chem. Phys.* **1989**, *91*, 2901.
(22) Biesner, J.; Schnieder, L.; Schmeer, J.; Ahlers, G.; Xie, X.; Welge, K. H.; Ashfold, M. N. R.; Dixon, R. N. *J. Chem. Phys.* **1988**, *88*, 3607.
(23) Xie, X.; Schnieder, L.; Wallmeier, H.; Boettner, R.; Welge, K. H.; Ashfold, M. N. R. *J. Chem. Phys.* **1990**, *92*, 1608.
(24) Schnieder, L.; Meier, W.; Welge, K. H.; Ashfold, M. N. R.; Western, C. M. *J. Chem. Phys.* **1990**, *92*, 7027.
(25) Ashfold, M. N. R.; Lambert, I. R.; Mordaunt, D. H.; Morley, G. P.; Western, C. M. *J. Phys. Chem.* **1992**, *96*, 2938.
(26) Morley, G. P.; Lambert, I. R.; Ashfold, M. N. R.; Rosser, K. N.; Western, C. M. *J. Chem. Phys.* **1992**, *97*, 3157.
(27) Mordaunt, D. H.; Lambert, I. R.; Morley, G. P.; Ashfold, M. N. R.; Dixon, R. N.; Western, C. M. *J. Chem. Phys.* **1993**, *98*, 2054.
(28) Ashfold, M. N. R.; Mordaunt, D. H.; Wilson, S. H. S. In *Advances in Photochemistry*; Neckart, D., Volman, D., van Bunar, G., Eds.; (Wiley: New York, in press).
(29) Mordaunt, D. H.; Ashfold, M. N. R.; Dixon, R. N. *J. Chem. Phys.* **1994**, *100*, 7360.
(30) Schnieder, L.; Seekamp-Rahn, K.; Liedeker, F.; Steuwe, H.; Welge, K. H. *Faraday Discuss. Chem. Soc.* **1991**, *91*, 259−269.
(31) Aoiz, F. J.; Bañares, L.; D'Mello, M. J.; Herrero, V. J.; Sáez Rábanos, V.; Schnieder, L.; Wyatt, R. E. *J. Chem. Phys.* **1994**, *101*, 5781.
(32) Schnieder, L.; Seekamp-Rahn, K.; Borkowski, J.; Wrede, E.; Welge, K. H.; Aoiz, F. J.; Bañares, L.; D'Mello, M. J.; Herrero, V. J.; Sáez Rábanos, V.; Wyatt, R. E. *Science* (*Washington, D.C.*), **1995**, *269*, 207.
(33) Siegbahn, P.; Liu, B. *J. Chem. Phys.* **1978**, *68*, 2457.
(34) Truhlar, D. G.; Horowitz, C. J. *J. Chem. Phys.* **1978**, *68*, 2466.
(35) Truhlar, D. G.; Horowitz, C. J. *J. Chem. Phys.* **1979**, *71*, 1514.
(36) Wu, Y. M.; Lepetit, B.; Kuppermann, A. *Chem. Phys. Lett.* **1991**, *186*, 319.
(37) Wu, Y. M.; Kuppermann, A. *Chem. Phys. Lett.* **1993**, *201*, 178.
(38) Kuppermann, A.; Wu, Y. M. *Chem. Phys. Lett.* **1993**, *205*, 577.
(39) Kuppermann, A.; Wu, Y. M. *Chem. Phys. Lett.* **1993**, *213*, 636.
(40) Kliner, D. A. V.; Adelman, D. E.; Zare, R. N. *J. Chem. Phys.* **1991**, *94*, 1069.
(41) Continetti, R. E.; Zhang, J. Z. H.; Miller, W. H. *J. Chem. Phys.* **1990**, *93*, 5356.
(42) Miller, W. H.; Zhang, J. Z. H. *J. Phys. Chem.* **1992**, *96*, 7767.
(43) Aoiz, F. J.; Herrero, V. J.; Sáez Rábbanos, V. *J. Chem. Phys.* **1992**, *97*, 7423.
(44) Kliner, D. A. V.; Adelman, D. E.; Zare, R. N. *J. Chem. Phys.* **1991**, *95*, 1648.
(45) Schultz, A.; Cruse, H. W.; Zare, R. N. *J. Chem. Phys.* **1972**, *57*, 1354; Dagdigian, P. J.; Zare, R. N.; *Science*, **1974**, *185*, 739.
(46) Collins, C. B.; Johnson, B. W.; Mirza, M. Y.; *Phys. Rev.* **1974**, *A10*, 813.
(47) Johnson, P. M.; Berman, M. R.; Zakheim, D. *J. Chem. Phys.* **1975**, *62*, 2500.
(48) Kinsey, J. L. *J. Chem. Phys.* **1977**, *66*, 2560.
(49) Cline, J. I.; Taatjes, C. A.; Leone, S. R. *J. Chem. Phys.* **1990**, *93*, 6543.
(50) Taatjes, C. A.; Cline, J. I.; Leone, S. R. *J. Chem. Phys.* **1990**, *93*, 6554.
(51) Simons, J. P. *J. Phys. Chem.* **1987**, *91*, 5378.
(52) Houston, P. L. *J. Phys. Chem.* **1987**, *91*, 5388−5397.
(53) Docker, M. P.; Hodgson, A.; Simons, J. P. In *Molecular Photodissociation Dynamics*; Ashfold, M. N. R., Baggott, J. E., Eds.; Royal Society Chemistry: London: 1987.
(54) Houston, P. L. *Acc. Chem. Res.* **1989**, *22*, 309−314.
(55) Hall, G. E.; Houston, P. L. *Annu. Rev. Phys. Chem.* **1989**, *40*, 375−405.
(56) Orr-Ewing, A. J.; Zare, R. N. *Annu. Rev. Phys. Chem.* **1994**, *45*, 315.
(57) Orr-Ewing, A. J.; Zare, R. N. In *Chemical Dynamics and Kinetics of Small Radicals*; Wagner, A.; Liu, K., Eds.; World Scientific: Singapore, 1995.
(58) Brouard, M.; Simons, J. P. In *Chemical Dynamics and Kinetics of Small Radicals*; Wagner, A., Liu, K., Eds.; World Scientific: Singapore, 1995).
(59) Gordon, R. J.; Hall, G. E. Applications of Doppler Spectroscopy in Photofragmentation. *Adv. Chem. Phys.*, in press.
(60) Schmiedl, R.; Dugan, H.; Meier, W.; Welge, K. H. *Z. Phys. A* **1982**, *304*, 137−142.
(61) Zare, R. N.; Herschbach, D. R. *Proc. IEEE* **1963**, *51*, 173.
(62) Zare, R. N. Ph.D. Thesis, Harvard University, Cambridge, MA, 1964.
(63) Ogorzalek, R.; Hall, G. E.; Härri, H.-P.; Houston, P. L. *J. Phys. Chem.* **1988**, *92*, 5−8.
(64) Xu, Z.; Koplitz, B.; Wittig, C. *J. Chem. Phys.* **1987**, *87*, 1062.
(65) Xu, Z.; Koplitz, B.; Wittig, C. *J. Chem. Phys.* **1989**, *90*, 2692.
(66) Dixon, R. N.; Nightingale, J.; Western, C. M.; Yang, X. *Chem. Phys. Lett.* **1988**, *151*, 328.
(67) Hall, G. E.; Sivakumar, N.; Houston, P. L.; Burak, I. *Phys. Rev. Lett.* **1986**, *56*, 1671−1674.
(68) Dixon, R. N. *J. Chem. Phys.* **1986**, *85*, 1866−1879.
(69) Dubs, M.; Brühlmann, U.; Huber, J. R. *J. Chem. Phys.* **1986**, *84*, 3106.
(70) Gericke, K.-H.; Klee, S.; Comes, F. J.; Dixon, R. N. *J. Chem. Phys.* **1986**, *85*, 4463.
(71) Docker, M. P.; Hodgson, A.; Simons, J. P. *Chem. Phys. Lett.* **1986**, *128*, 264.
(72) Klee, S.; Gericke, K.-H.; Comes, F. J. *J. Chem. Phys.* **1986**, *85*, 40.
(73) Gericke, K.-H.; Grunewald, A. U.; Klee, S.; Comes, F. J. *J. Chem. Phys.* **1988**, *88*, 6255.
(74) Klee, S.; Gericke, K. H.; Comes, F. J. *Ber. Bunsen-Ges. Phys. Chem.* **1988**, *92*, 429.
(75) Docker, M. P.; Hodgson, A.; Simons, J. P. *Faraday Discuss. Chem. Soc.* **1986**, *82*, 25.
(76) August, J.; Brouard, M.; Docker, M. P.; Hodgson, A.; Milne, C. J.; Simons, J. P. *Ber. Bunsen-Ges. Phys. Chem.* **1988**, *92*, 264.
(77) Grunewald, A. U.; Gericke, K.-H.; Comes, F. J. *Chem. Phys. Lett.* **1986**, *132*, 121.
(78) Grunewald, A. U.; Gericke, K.-H.; Comes, F. J. *J. Chem. Phys.* **1987**, *87*, 579.
(79) Grunewald, A. U.; Gericke, K.-H.; Comes, F. J. *J. Chem. Phys.* **1987**, *89*, 345.
(80) Comes, F. J.; Gericke, K.-H.; Grunewald, A. U.; Klee, S. *Ber. Bunsen-Ges. Phys. Chem.* **1988**, *92*, 273.
(81) Bergmann, K.; Hefter, U.; Witt, J. *J. Chem. Phys.* **1980**, *72*, 4777.
(82) Gottscho, R. A.; Field, R. W.; Bacis, R.; Silvers, S. J. *J. Chem. Phys.* **1980**, *73*, 599.
(83) McCaffery, A. J.; Reid, K. L.; Whitaker, B. J. *Phys. Rev. Lett.* **1988**, *61*, 2085.
(84) Fell, C. P.; McCaffery, A. J.; Reid, K. L.; Ticktin, A. *J. Chem. Phys.* **1991**, *95*, 4948.
(85) Reid, K. L.; McCaffery, A. J. *J. Chem. Phys.* **1991**, *95*, 4958.

(86) Collins, T. L. D.; McCaffery, A. J.; Richardson, J. P.; Wilson, R. J.; Wynn, M. J. *J. Chem. Phys.* **1995**, *102*, 4419.
(87) Collins, T. L. D.; McCaffery, A. J.; Wynn, M. J. *Phys. Rev. Lett.* **1991**, *66*, 137.
(88) Murphy, E. J.; Brophy, J. H.; Arnold, G. S.; Dimpfl, W. L.; Kinsey, J. L. *J. Chem. Phys.* **1979**, *70*, 5910.
(89) Murphy, E. J.; Brophy, J. H.; Kinsey, J. L. *J. Chem. Phys.* **1981**, *74*, 331.
(90) Serri, J. A.; Becker, C. H.; Elbel, M. B.; Kinsey, J. L.; Moskowitz, W. P.; Pritchard, D. E. *J. Chem. Phys.* **1981**, *74*, 5116.
(91) Hershberger, J. R.; Chou, J. Z.; Flynn, G. W.; Weston, R. E. *Chem. Phys. Lett.* **1988**, *149*, 51.
(92) Hershberger, J. R.; Hewitt, S. A.; Sakar, S. S.; Flynn, G. W.; Weston, R. E. *J. Chem. Phys.* **1989**, *91*, 4636.
(93) Kahn, F. A.; Kreutz, T. G.; Flynn, G. W.; Weston, R. E. *J. Chem. Phys.* **1990**, *92*, 4876.
(94) Chawla, G. K.; McBane, G. C.; Houston, P. L.; Schatz, G. C. *J. Chem. Phys.* **1988**, *88*, 5481.
(95) McBane, G. C. Ph.D. Thesis, Cornell University, Ithaca, NY, 1990.
(96) Shafer, N. E.; Orr-Ewing, A. J.; Simpson, W. R.; Xu, H.; Zare, R. N. *Chem. Phys. Lett.* **1993**, *212*, 155.
(97) Johnson, G. W.; Satyapal, S.; Bersohn, R.; Katz, B. *J. Chem. Phys.* **1990**, *92*, 206.
(98) Chattopadhyay, A.; Tasaki, S.; Bersohn, R.; Kawasaki, M. *J. Chem. Phys.* **1991**, *95*, 1033.
(99) Katz, B.; Park, J.; Satyapal, S.; Tasake, S.; Chattopadhyay, A.; Yi, W.; Bersohn, R. *Faraday Discuss. Chem. Soc.* **1991**, *91*, 73.
(100) Kim, H.-L.; Wickramaaratchi, M. A.; Zheng, X.; Hall, G. E. *J. Chem. Phys.* **1994**, *101*, 2033.
(101) Schafer, N. E. Ph.D. Thesis, Columbia University, New York, NY, 1990.
(102) Green, F.; Hancock, G.; Orr-Ewing, A. J.; Brouard, M.; Duxon, S. P.; Enriquez, P. A.; Sayos, R.; Simons, J. P. *Chem. Phys. Lett.* **1991**, *182*, 58.
(103) Green, F.; Hancock, G.; Orr-Ewing, A. J. *Faraday Discuss. Chem. Soc.* **1991**, *95*, 79.
(104) Brouard, M.; Duxon, S. P.; Enriquez, P. A.; Simons, J. P. *J. Chem. Phys.* **1991**, *95*, 8169.
(105) King, D. S.; Saunder, D. G.; Casassa, M. P. *J. Chem. Phys.* **1992**, *97*, 5919.
(106) Brouard, M.; Duxon, S. P.; Enriquez, P. A.; Simons, J. P. *J. Chem. Phys.* **1992**, *97*, 7414.
(107) Aoiz, F. J.; Brouard, M.; Enriquez, P. A.; Sayos, R. *J. Chem. Soc., Faraday Trans.* **1993**, *89*, 1427.
(108) Brouard, M.; Duxon, S. P.; Enriquez, P. A.; Simons, J. P. *J. Chem. Soc., Faraday Trans.* **1993**, *89*, 1435.
(109) Simpson, W. R.; Orr-Ewing, A. J.; Zare, R. N. *Chem. Phys. Lett* **1993**, *212*, 163.
(110) Costen, M. L.; Hancock, G.; Orr-Ewing, A. J.; Summerfield, D. *J. Chem. Phys.* **1994**, *100*, 2754.
(111) Shafer, N. E.; Xu, H.; Tuckett, R. P.; Springer, M.; Zare, R. N. *J. Phys. Chem.* **1994**, *98*, 3369.
(112) Meyer, H. *Chem. Phys. Lett.* **1994**, *230*, 519.
(113) Meyer, H. *J. Phys. Chem.* **1995**, *99*, 1101.
(114) Meyer, H. *Mol. Phys.* **1995**, *84*, 1155.
(115) Meyer, H. *J. Chem. Phys.* **1995**, *102*, 3151−68.
(116) Tomer, J. L.; Wall, M. C.; Reid, B. P.; Cline, J. I. *Chem. Phys. Lett.* **1993**, *216*, 286.
(117) Uberna, R.; Cline, J. I. *J. Chem. Phys.* **1995**, *102*, 4705.
(118) Tomer, J. L.; Wall, M. C.; Reid, B. P.; Cline, J. I. *J. Chem. Phys.* **1995**, *102*, 6100.
(119) Uberna, R.; Hinchliffe, R. D.; Cline, J. I. NO $\mu-\mathbf{v}-\mathbf{J}$ correlation in the photofragmentation of 2-chloro-2-nitrosopropane, in press.
(120) Uberna, R.; Hinchliffe, R. D.; Cline, J. I. Photofragment $\mu-\mathbf{v}-\mathbf{J}$ correlation Measured by $1 + n'$ resonance-enhanced multiphoton ionization: selective probing of bipolar moments and detection of chiral dynamics. *J. Chem. Phys.*, in press.
(121) Chen, K.-M. *Chem. Phys. Lett.* **1992**, *198*, 288.
(122) Chen, K.-M.; Pei, C.-C. *Chem. Phys. Lett.* **1994**, *217*, 471.
(123) Chen, K.-M.; Kuo, C.-N.; Tzeng, M.-H.; Shian, M.-L.; Chung, S.-E. *Chem. Phys. Lett.* **1994**, *221*, 341.
(124) Tonokura, K.; Suzuki, T. *Chem. Phys. Lett.* **1994**, *224*, 1.
(125) Chandler, D. W.; Houston, P. L. *J. Chem. Phys.* **1987**, *87*, 1445−1447.
(126) de Bruijn, D. P.; Los, J. *Rev. Sci. Instrum.* **1982**, *53*, 1020−1026.
(127) Brenot, J. C.; Durup-Ferguson, M. In *State-Selected and State-to-State Ion-Molecule Reaction Dynamics, Part 1: Experiment*; Ng, C. Y.; Baer, M., Eds, Wiley: New York, 1992; pp 309−399.
(128) Heck, A. J. R.; Chandler, D. W. *Annu. Rev. Phys. Chem*, **1995**, *46*, 335−372.
(129) Houston, P. L. *Acc. Chem. Res.* **1995**, *28*, 453−460.
(130) Kang, W. K.; Kim, Y. S.; Jung, K.-H. *Chem. Phys. Lett.* **1995**, *244*, 183.
(131) Umemoto, M.; Seki, K.; Shinohara, H.; Nagashima, U.; Nishi, N.; Kinoshita, M.; Shimada, R. *J. Chem. Phys.* **1985**, *83*, 1657−66.
(132) Mo, Y.; Tonokura, K.; Matsumi, Y.; Kawasaki, M.; Sato, T.; Arikawa, T.; Reilly, P. T. A.; Xie, Y.; Yang, Y. A.; *et al. J. Chem. Phys.* **1992**, *97*, 4815−26.
(133) Huang, Y.; Yang, Y.-A.; He, G.; Hashimoto, S.; Gordon, R. J. *J. Chem. Phys.* **1995**, *103*, 5476−87.
(134) Suzuki, T.; Tonokura, K.; Bontuyan, L. S.; Hashimoto, N. *J. Phys. Chem.* **1994**, *98*, 13447.
(135) Suzuki, T. Private communication.
(136) Kitsopoulos, T. N.; Buntine, M. A.; Baldwin, D. P.; Zare, R. N.; Chandler, D. W. *Science* (*Washington, D.C.*) **1993**, *260*, 1605−1610.
(137) Martin, C. P.; Jelinsky, P.; Lampton, M.; Malina, R. F.; Anger, H. O. *Rev. Sci. Instrum.* **1989**, *52*, 1051.
(138) Hanold, K. A.; Sherwood, C. R.; Continetti, R. E. *J. Chem. Phys.* **1995**, *103*, 9876−9879.
(139) Hanold, K A.; Sherwood, C. R.; Garner, M. C.; Continetti, R. E. *Rev. Sci. Instrum.* **1995**, *66*, 5507−5511.
(140) Cyr, D. R.; Continetti, R. E.; Metz, R. B.; Osborn, D. L.; Neumark, D. M. *J. Chem. Phys.* **1992**, *97*, 4937.
(141) Leahy, D. J.; Cyr, D. R.; Osborn, D. L.; Neumark, D. M. *Chem. Phys. Lett.* **1993**, *216*, 503.
(142) Cyr, D. R.; Leahy, D. J.; Osborn, D. L.; Continetti, R. E.; Neumark, D. M. *J. Chem. Phys.* **1993**, *99*, 8751.
(143) Leahy, D. J.; Cyr, D. R.; Osborn, D. L.; Neumark, D. M. *Proc. SPIE* **1993**, *1858*, 49.
(144) Continetti, R. E.; Cyr, D. R.; Osborn, D. L.; Leahy, D. J.; Neumark, D. M. *J. Chem. Phys.* **1993**, *99*, 2616.
(145) Osborn, D. L.; Leahy, D. J.; Ross, E. M.; Neumark, D. M. *Chem. Phys. Lett.* **1995**, *235*, 484.
(146) Leahy, D. J.; Osborn, D. L.; Cyr, D. R.; Neumark, D. M. *J. Chem. Phys.* **1995**, *103*, 2495−2508.
(147) Sherwood, C. R.; Garner, M. C.; Hanold, K. A.; Strong, K. M.; Continetti, R. E. *J. Chem. Phys.* **1995**, *102*, 6949.
(148) Garner, M. C.; Sherwood, C. R.; Hanold, K. A.; Continetti, R. E. Submitted.
(149) Corr, D.; Jacobs, D. C. *Rev. Sci. Instrum.* **1992**, *63*, 1969.
(150) Martin, J. S.; Greeley, J. N.; Morris, J. R.; Feranchak, B. T.; Jacobs, D. C. *J. Chem. Phys.* **1994**, *100*, 6791.
(151) Greeley, J. N.; Martin, J. S.; Morris, J. R.; Jacobs, D. C. *J. Chem. Phys.* **1995**, *102*, 4996.
(152) Morris, J. R.; Martin, J. S.; Greeley, J. N.; Jacobs, D. C. *Surf. Sci.* **1995**, *330*, 323.
(153) Menges, M.; Baumeister, B.; Al-Shamery, K.; Freund, J.-J.; Fischer, C.; Andresen, P. *Surf. Sci.* **1994**, *316*, 103.
(154) Sugawara, K.; Sun, W.; Wach, Th.; Wanner, J. *Ber. Bunsen-Ges. Phys. Chem.* **1995**, *99*, 1357.
(155) Jones, A. B.; Buxey, A. L. M.; Jukes, P. R.; Smith, J. A.; Stace, A. J. *J. Chem. Phys.* **1995**, *103*, 474.
(156) Hertz, R. A.; Syage, J. A. *J. Chem. Phys.* **1994**, *100*, 9265.
(157) Syage, J. A. *J. Phys. Chem.* Submitted.
(158) Chen, K.-M.; Sung, C.-H.; Chang, J.-L.; Chung, T.-H.; Lee, K.-H. *Chem. Phys. Lett.* **1995**, *240*, 17.
(159) Chen, K.-M.; Chang, J.-L.; Sung, C.-H.; Chung, T.-H.; Lee, K.-H. *Proc. Proc. SPIE* **1995**, *2548*, 115.
(160) Chen, K.-M.; Lee, K.-H.; Chang, J.-L.; Sung, C.-H.; Chung, T.-H.; Liu, T.-K.; Perng, H.-C. *J. Phys. Chem.* submitted.
(161) Ni, H.; Serafin, J. M.; Valentini, J. J. *Chem. Phys. Lett.* **1995**, *244*, 207.
(162) Sanov, A.; Bieler, C. R.; Reisler, H. *J. Phys. Chem.* **1995**, *99*, 13637.
(163) Stolte, S. *Ber. Bunsen-Ges. Phys. Chem.* **1982**, *86*, 413.
(164) Zare, R. N. *Ber. Bunsen-Ges. Phys. Chem.* **1982**, *86*, 422.
(165) Parker, D. H.; Bernstein, R. B. *Annu. Rev. Phys. Chem.* **1989**, *40*, 561.
(166) Brooks, P. R. *Science* (*Washington, D.C.*) **1976**, *193*, 11.
(167) Kasai, T.; Fukawa, T.; Matsunami, T.; Che, D.-C.; Ohashi, K.; Fukunishi, Y.; Ohoyama, H.; Kuwata, K. *Rev. Sci. Instrum.* **1993**, *64*, 1150.
(168) Kuwata, K.; Kasai, T. Steric Effects in Small Radical Formations In *Chemical Dynamics and Kinetics of Small Radicals*; Wagner, A.; Liu, K., Eds.; World Scientific: Singapore, 1995.
(169) Leone, S. R. *Annu. Rev. Phys. Chem.* **1984**, *35*, 109.
(170) Leone, S. R. *Acc. Chem. Res.* **1992**, *25*, 71.
(171) Loesch, H. J. *Annu. Rev. Phys. Chem.* **1995**, *46*, 555−594.
(172) *J. Phys. Chem.* **1987**, *91*, 5365−5515 (Dynamical Aspects of Stereochemistry issue).
(173) *J. Phys. Chem.* **1991**, *95*, 7961−8421 (Richard Bernstein Memorial Issue on Molecular Dynamics).
(174) *J. Phys. Chem.* **1995**, *99*, 13569−13754 (Stereodynamics and Active Control issue).
(175) Proceedings of Faraday Symposium Number 24, Orientation and Polarisation Effects in Reactive Collisions. *J. Chem. Soc., Faraday Trans. 2* **1989**, *85* (8).
(176) Karny, Z.; Estler, R. C.; Zare, R. N. *J. Chem. Phys.* **1978**, *69*, 5199.

(177) McKendrick, K. G. *J. Chem. Soc., Faraday Trans. 2* **1989**, *85*, 1284−1285.
(178) Zhang, R.; Rakestraw, D. J.; McKendrick, K. G.; Zare, R. N. *J. Chem. Phys.* **1989**, *89*, 6283−6294.
(179) Loesch, H. J.; Steinkemeier, F. *J. Chem. Phys.* **1994**, *100*, 740−743.
(180) Pullman, D. P.; Friedrich, B.; Herschbach, D. R. *J. Chem. Phys.* **1990**, *93*, 3224.
(181) Friedrich, B.; Pullman, D. P.; Herschbach, D. R. *J. Phys. Chem.* **1991**, *95*, 8118.
(182) Friedrich, B.; Herschbach, D. R. *Nature* **1991**, *353*, 412.
(183) Taatjes, C. A.; Janssen, M. H. M.; Stolte, S. *Chem. Phys. Lett.* **1993**, *203*, 363.
(184) Mastenbroek, J. W. G.; Taatjes, C. A.; Nauta, K.; Janssen, M. H. M.; Stolte, S. *J. Phys. Chem.* **1995**, *99*, 4360.
(185) Mastenbroek, J. W. G.; Nauta, B. K.; Janssen, M. H. M.; Stolte, S. *Proc. SPIE* **1995**, *2548*, 39−48.
(186) Bazalgette, G.; White, R.; Loison, J. C.; Trénec, G.; Vigué, J. *Chem. Phys. Lett.* **1995**, *244*, 195.
(187) Kim, D. Y.; Brandstater, N.; Pipes, L.; Garner, T.; Baugh, D. *J. Phys. Chem.* **1995**, *99*, 4364.
(188) Choi, S. E.; Bernstein, R. B. *J. Chem. Phys.* **1985**, *83*, 4463.
(189) Loesch, H. J.; Remscheid, A. *J. Chem. Phys.* **1990**, *93*, 4779.
(190) Loesch, H. J.; Remscheid, A. *J. Phys. Chem.* **1991**, *95*, 8194.
(191) See also in this issue: Miller, R.; Bacic, Z Clusters: Dynamics and Structure of Weakly Bound Systems. *J. Phys. Chem.* **1996**, *100*, 12945.
(192) Jouvet, C.; Boivineaau, M.; Duval, M. C.; Soep, B. *J. Phys. Chem.* **1987**, *91*, 5416.
(193) Breckenridge, W. H. *Acc. Chem. Res.* **1989**, *22*, 21.
(194) Breckenridge, W. H.; Duval, M. C.; Jouvet, C.; Soep, B. In *Structure and Dynamics of Weakly Bound Molecular Complexes*; Weber, A., Ed.; D. Reidel: Amsterdam, 1987; p. 213.
(195) Wittig, C.; Sharpe, S.; Beaudet, R. A. *Acc. Chem. Res.* **1988**, *21*, 341−347.
(196) Chen, Y.; Hoffmann, F.; Shin, S. K.; Oh, D.; Sharpe, S.; Zeng, Y. P.; Beaudet, R. A.; Wittig, C. *Adv. Mol. Vib. Collision Dyn.* **1991**, *1B*, 187−229.
(197) Shin, S. K.; Chen, Y.; Nickolaisen, S.; Sharpe, S. W.; Beaudet, R. A.; Wittig, C. *Adv. Photochem.* **1991**, *16*, 249−363.
(198) Wittig, C.; Zewail, A. H.; Dynamics of Ground-State Bimolecular Reactions. In *Chemical Reactions in Clusters;* Bernstein, E. R., Ed.; Oxford University Press: Oxford, 1996.
(199) Sharpe, S. W.; Zeng, Y. P.; Wittig, C.; Beaudet, R. A. *J. Chem. Phys.* **1990**, *92*, 943.
(200) Zeng, Y. P.; Sharpe, S. W.; Shin, S. K.; Wittig, C.; Beaudet, R. A. *J. Chem. Phys.* **1992**, *97*, 5392.
(201) Wittig, C.; Engel, Y. M.; Levine, R. D. *Chem. Phys. Lett.* **1988**, *153*, 411.
(202) For further discussion of this type of experiment, see the article by A. H. Zewail in this issue.
(203) Scherer, N. F.; Khundkar, L. R.; Bernstein, R. B.; Zewail, A. H. *J. Chem. Phys.* **1990**, *87*, 1451.
(204) Jouvet, C.; Soep, B. *Laser Chem.* **1985**, *5*, 157.
(205) Breckenridge, W. H.; Jouvet, C.; Soep, B. *J. Chem. Phys.* **1986**, *84*, 1443.
(206) Breckenridge, W. H.; Jouvet, C.; Duval, M. C.; Soep, B. *J. Chim. Phys. Phys.-Chim. Biol.* **1987**, *64*, 381.
(207) Ionov, S. I.; Brucker, G. A.; Jaques, C.; Valachovic, L.; Wittig, C. *J. Chem. Phys.* **1992**, *97*, 9486.
(208) Ionov, S. I.; Brucker, G. A.; Jaques, C.; Valachovic, L.; Wittig, C. *J. Chem. Phys.* **1993**, *99*, 6553.
(209) Neumark, D. M. Transition state spectroscopy of bimolecular chemical reactions. *Annu. Rev. Phys. Chem.* **1992**, *43*, 153−176.
(210) Metz, R. B.; Bradforth, S. E.; Neumark, D. M. *Adv. Chem. Phys.* **1992**, *81*, 1−61.
(211) Neumark, D. M. *Acc. Chem. Res.* **1993**, *26*, 33−40.
(212) Bradforth, S. E.; Weaver, A.; Arnold, D. W.; Metz, R. B.; Neumark, D. M. *J. Chem. Phys.* **1990**, *92*, 7205.
(213) Bradforth, S. E.; Arnold, D. W.; Neumark, D. M.; Manolopoulos, D. E. *J. Chem. Phys.* **1993**, *99*, 6345.
(214) Manolopoulos, D. E.; Stark, K.; Werner, H. J.; Arnold, D. W.; Bradforth, S. E.; Neumark, D. M. *Science* (*Washington, D.C.*) **1993**, *262*, 1852.
(215) Case, D. A.; McClelland, G. M.; Herschbach, D. R. *Mol. Phys.* **1978**, *35*, 541.
(216) Berman, P. R. *J. Quant. Spectrosc. Radiat. Transfer* **1972**, *12*, 1331.
(217) Berman, P. R. *Adv. Atom. Mol. Phys.* **1978**, *13*, 57.
(218) Phillips, W. D.; Pritchard, D. *Phys. Rev. Lett.* **1974**, *33*, 1254.
(219) Apt, J.; Pritchard, D. E. *Phys. Rev. Lett.* **1976**, *37*, 91.
(220) Smith, N.; Brunner, T. A.; Pritchard, D. E. *J. Chem. Phys.* **1981**, *74*, 467.
(221) Smith, N.; Scott, T. P.; Pritchard, D. E. *J. Chem. Phys.* **1984**, *81*, 1229.
(222) O'Callaghan, M. J.; Cooper, J. *Phys. Rev. A* **1989**, *39*, 6206.
(223) Liu, W.-K.; Dickinson, A. S. *J. Phys. B* **1991**, *24*, 1259.
(224) Collins, T. L. D.; McCaffery, A. J.; Wynn, M. J. *Faraday Discuss Chem. Soc.* **1991**, *91*, 91.
(225) McCaffery, A. J.; Reid, K. L.; Whitaker, B. J. *Phys. Rev. Lett.* **1988**, *61*, 2085.
(226) Collins, T. L. D.; McCaffery, A. J.; Richardson, J. P.; Wynn, M. J. *Phys. Rev. Lett.* **1993**, *70*, 3392.
(227) Greenfield, E.; Gao, Y.; Stewart, B. Absolute Velocity-dependent Inelastic Cross Sections from Double-resonance Lineshapes. *Phys. Rev. Lett.*, submitted.
(228) Collins, T. L. D.; McCaffery, A. J.; Wynn, M. J. *Phys. Rev. Lett.* **1991**, *66*, 137.
(229) Johnston, G. W.; Satyapal, S.; Bersohn, R.; Katz, B. *J. Chem. Phys.* **1990**, *96*, 206.
(230) Green, F.; Hancock, G.; Orr-Ewing, A. J.; Brouard, M.; Duxon, S. P.; Enriquez, P. A.; Sayos, R.; Simons, J. P. *Chem. Phys. Lett.* **1991**, *182*, 569.
(231) Brouard, M.; Duxon, S. P.; Enriquez, P. A.; Simon, J. P. *J. Chem. Phys.* **1992**, *97*, 7414.
(232) Casassa, M. P.; Sauder, D. G.; King, D. S. *Proc. SPIE* **1992**, *1858*, 256.
(233) King, D. S.; Sauder, D. G.; Casassa, M. P. *J. Chem. Phys.* **1992**, *97*, 5919.
(234) Aoiz, F. J.; Brouard, M.; Enriquez, P. A.; Sayos, R. *J. Chem. Soc., Faraday Trans.* **1993**, *XX*, xxxx.
(235) Costen, M. L.; Hancock, G.; Orr-Ewing, A. J.; Summerfield, D. *J. Chem. Phys.* **1994**, *100*, 2754−2764.
(236) Brouard, M.; Duxon, S. P.; Enriquez, P. A.; Simons, J. P. *J. Chem. Soc., Faraday Trans.* **1993**, *XX*, xxxx.
(237) Shafer-Rae, N. E.; Orr-Ewing, A. J.; Zare, R. N. *J. Phys. Chem.* **1995**, *99*, 7591.
(238) Xu, H.; Shafer-Ray, N. E.; Merkt, F.; Hughes, D. J.; Springer, M.; Tuckett, R. P.; Zare, R. N. *J. Chem. Phys.* **1995**, *103*, 5157.
(239) Simpson, W. R.; Orr-Ewing, A. J.; Zare, R. N. *Chem. Phys. Lett.* **1993**, *212*, 163.
(240) Simpson, W. R.; Orr-Ewing, A. J.; Rakitzis, T. P.; Kandel, S. A.; Zare, R. N. *J. Chem. Phys.* **1995**, *103*, 7299.
(241) Simpson, W. R.; Rakitzis, T. P.; Kandel, S. A.; Orr-Ewing, A. J; Zare, R. N. *J. Chem. Phys.* **1995**, *103*, 7313.
(242) Brouard, M.; Lambert, H. M.; Russell, C. L.; Short, J.; Simons, J. P. *Faraday Discuss. Chem. Soc.* **1995**, *102*, xxxx.
(243) Alexander, A. J.; Brouard, M.; Rayner, S. P.; Simons, J. P. *Chem. Phys.* (Special Issue), in press.

JP960131F